THE ROYAL SOCIETY

X-ray topography studies of microdefects in silicon

By Grzegorz Kowalski, Maria Lefeld-Sosnowska, Jerzy Gronkowski and Janusz Borowski

Institute of Experimental Physics, University of Warsaw, Hoza 69, 00-681 Warsaw, Poland

X-ray topography has been successfully applied to study microdefects with sizes in the range from well below standard topographic resolution to tenths of a μm, thus effectively widening the applicability of Lang section topography. The lower value is set by the application of high-order asymmetric reflections. The disappearance of the Kato fringes on section topographs is a clear indication of the existence of defects which are not detectable as standard contrast features. The presence of defects with such sizes was confirmed by transmission electron microscopy. Microdefects in the higher end of the size spectrum are well covered by Lang traverse and section topography, where detailed study of the contrast is possible for individual defects. Lang traverse and section topographies were applied to study specific cases of oxygen-related defects in silicon crystals.

Keywords: X-ray topography; diffraction lattice; defects; silicon

1. Introduction

The electronics industry is the main consumer of semiconductor materials such as silicon (Si), gallium arsenide (GaAs) and fabrication of electronic devices involves use of complex chemical, physical and thermal processes. At all stages of fabrication (including growth of the substrate crystals), crystal-lattice defects are likely to be introduced. Silicon single crystals (as manufactured today) are already free from large defects, such as dislocations, but point defects and their aggregates are still present. Some of the defects are non-intentional and some are connected with intentional dopants used during the processing. Techniques like defect gettering create regions that act as sinks for unwanted crystal-lattice defects. The size of the defects can vary from a single atom to micrometre-sized precipitates. Relevant experimental techniques may record and visualize most of them. X-rays can offer, in this respect, a wide range of tools, including multi-crystal high-resolution diffractometers to study statistically distributed point-like defects on the atomic scale, as well as topographic techniques dealing with micrometre-sized aggregates. X-ray topography is non-destructive and comprehensive in mapping whole crystal slices. The term 'X-ray topograph' was coined by Ramachandran (1944), but the technique was really developed to its present status by Lang (1957, 1958, 1959*a*, *b*). Section topography (Lang 1957) and traverse topography (Lang 1958, 1959*a*, *b*) were, and still are, widely used for the investigation of microdefects in various crystals, especially in silicon. Both of Lang's techniques were extensively used to detect and image point

defects and their agglomerations, known as 'swirls' in as-grown floating zone silicon (Fz Si) (De Kock 1970, 1973; De Kock & van de Wijgert 1980*a*, *b*; De Kock *et al*. 1974, 1975*a*, *b*, 1979; Roksnoer *et al*. 1976; Roksnoer & van de Boom 1981; Roksnoer 1984; Föll *et al*. 1981). The topographical studies of annealed Czochralski-grown silicon (Cz Si) (Matsui & Kawamura 1972; Patel 1973) started after observations made by Patel & Batterman (1963), where a strong decrease in the X-ray anomalous transmission intensity in the dislocation-free (but oxygen-containing) annealed silicon crystals was recorded. A significant number of papers were and still are devoted to investigations of the oxygen-related microdefects by X-ray section and traverse topography (Patel & Authier 1975; Freeland *et al*. 1977; Patel *et al*. 1977; Chikawa & Shirai 1977; Patrick *et al*. 1979; Kishino *et al*. 1979; Yamamoto *et al*. 1980; Sugita *et al*. 1987; Iida *et al*. 1988, 1990, 1998; Stephenson 1990, 1992; Li *et al*. 1994; Lefeld-Sosnowska 1985; Lefeld-Sosnowska *et al*. 1988, 1995, 1996*a*, *b*; Lefeld-Sosnowska & Gronkowski 1989; Green *et al*. 1990; Holland *et al*. 1991; Okitsu *et al*. 1992; Mai *et al*. 1990). Many aspects of oxygen precipitation in Cz Si have been extensively studied in the last 20 years by many authors (for a review see Borghesi *et al*. (1995) and references therein).

Dislocation-free Czochralski-grown silicon crystals may contain interstitial oxygen atoms (O_i) with concentrations of 10^{17}–10^{18} cm^{-3}, dissolved from the quartz crucible and incorporated during the growth. In the process of fabrication of integrated circuits at high temperatures, agglomeration of O_i atoms may lead to the formation of silicon oxide precipitates and microdefects. The oxygen-related microdefects formed in the surface layer of the crystal have a detrimental effect on the yield of integrated circuits fabricated on Cz Si. On the other hand, oxide precipitates and microdefects formed in the bulk of the crystal can play a positive role; they getter the unwanted impurities from the electrically active regions of the junction. In the near-surface region of the crystal, the so-called denuded zone can be formed during a three-step high-temperature annealing process. The first anneal at 1373–1473 K causes the outgassing of oxygen from the surface layer. Then, at 873–1073 K, nucleation of oxygen precipitates is initiated, and finally, again at a high temperature (1273–1323 K), further growth of precipitates, involving transformation of their shapes and generation of microdefects, takes place (Zulehner 1989; Yang *et al*. 1987).

The type, shape, dimensions and concentrations of the precipitates and microdefects formed during annealing processes depend mainly on the temperature and duration of the annealing as well as on the thermal history of the sample during its growth. The latter determines the concentration and distribution of oxygen atoms and other impurities (Zulehner 1989).

The processes of nucleation and precipitation of oxygen, as well as the structure of microdefects formed in Cz Si, have been investigated mainly after one-step or two-step annealing (Borghesi *et al*. 1995; Zulehner 1989; Kung 1989; Lefeld-Sosnowska *et al*. 1995). However, multi-step annealing has also been applied in order to introduce oxygen-related microdefects in heavily doped silicon wafers for the purpose of intrinsic gettering (Rozgonyi & Jaccodine 1983; Tsuya *et al*. 1983).

2. Topography techniques

Single crystals containing microdefects with diameters smaller then a few μm present a specific challenge for the X-ray experiment. The resolution limit for a topographic

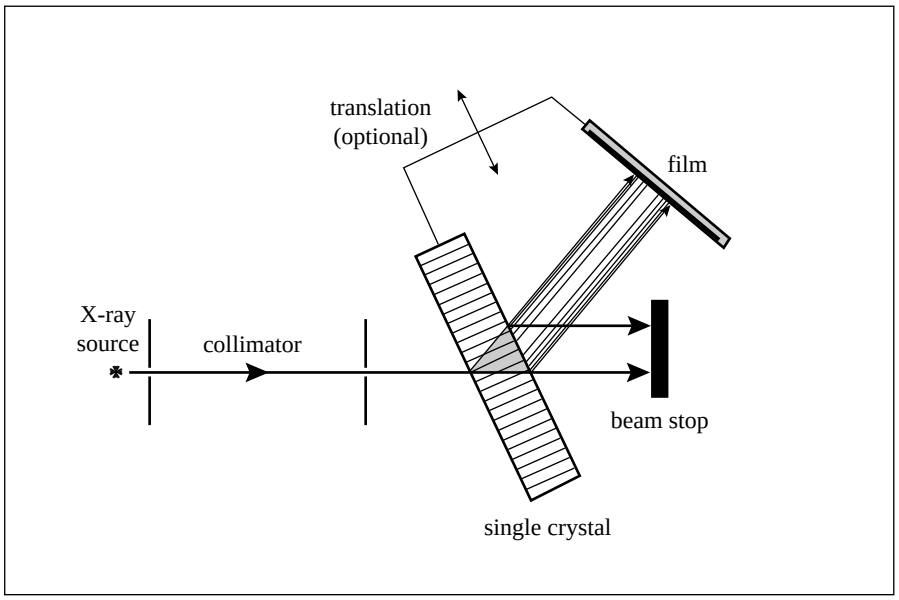

Figure 1. Schematic configuration of the experimental set-up for Lang section and traverse topography. When the film holder and crystal under study are translated on the common platform across the incoming X-ray beam, it represents the Lang traverse topography configuration. When crystal and film holder are stationary we see the classic section topography set-up.

method employing photographic emulsion is set by the grain size of the emulsion itself. Ilford nuclear emulsion type L4, with grains *ca.* 0.2 μm in size, is still not matched by the resolution achieved in any electronic system. The best line resolution achieved by the X-ray topography method is of the order of 1000 lines mm^{-1}, whereas point resolution is around 1 μm. It depends, of course, on the quality of dark-room techniques. X-ray section topography (Lang 1957) is the simplest X-ray topographic technique for imaging crystal-lattice defects (figure 1), and it is also the best understood theoretically.

The usefulness of the technique for the study of microdefects in silicon crystals (or any other crystals in this respect) has been demonstrated by many authors. Analysis of the results of section topography experiments can be supported by computer-simulated images of relevant defects, thus enabling a detailed examination of all important parameters (fault vectors, strain fields, etc.). For example, such studies for oxygen-related microdefects and precipitates in silicon were done by Patel & Authier (1975), Green *et al.* (1990), Holland *et al.* (1991), Holland & Tanner (1995) and Lefeld-Sosnowska *et al.* (1989). (Part of figure 2 is taken from this last work.)

The diffraction contrast due to the microdefects, recorded on section topographs, depends on the extent of their strain field and their position inside the crystal with respect to the X-ray incoming beam. Very small microdefects (on the verge of detectability on X-ray topographs) give only simple direct contrast, without any fine structure. The image of spherical microdefects when fully developed (usually for diameters of the order of several tenths of a μm) consists of direct contrast (black head), dynamic contrast (white tail) with fine structure due to intermediary contrast

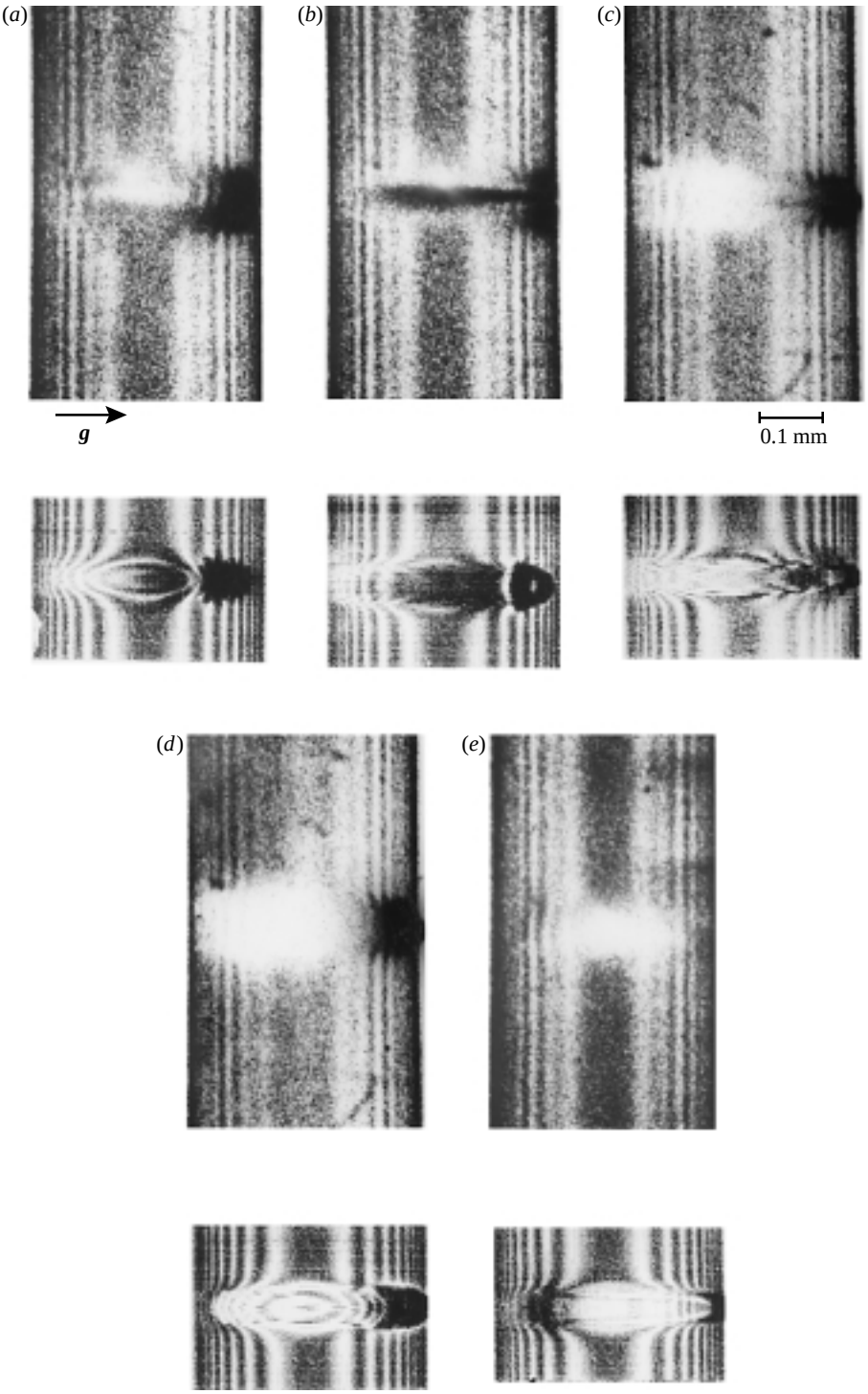

Figure 2. For description see opposite.

(Green *et al*. 1990; Holland & Tanner 1995). The specific features of this contrast depend on the physical parameters characterizing the defect, such as the fault vector, the magnitude and sign of the strain field, as well as the geometry of the defect and its position inside the Borrmann triangle (Green *et al*. 1990; Holland & Tanner 1995).

Traverse topography (Lang 1959*a*, *b*) can be extremely useful in assessing the distribution of lattice defects in large-area samples and, in particular, microdefects of sufficient size to be imaged. Figure 3 is an example of SiO_2 precipitates in silicon crystals after a two-step annealing process. Density, average size and associated strain fields can be easily deduced from such an experiment.

The diffraction contrast of large spherical precipitates consists of two semi-rings divided by a line of no contrast (Authier 1975; Tanner 1976; Bowen & Tanner 1998; Jung & Lefeld-Sosnowska 1984). When specific conditions are met, prismatic dislocation loops of hexagonal shape are formed during thermal treatment. They exhibit specific contrast where only a dislocation line is imaged with no contrast inside (Patel & Authier 1975). If the dislocation loop bounds the stacking fault (SF) plane, strong contrast inside the loop due to the presence of SF is clearly seen (Patel & Authier 1975; Matsui & Kawamura 1972). An example of this type of contrast is shown in figure 3 (already reported by Lefeld-Sosnowska *et al*. (1995)).

3. Application to silicon crystals

(*a*) *Samples*

In order to find the most favourable conditions for oxygen precipitation, two kinds of three-step annealing with different nucleation processes were applied (Surma 1988). The aim of the present work is to characterize defects formed in Si wafers during such procedures. We have chosen only three samples from a larger pool for this presentation, and only selected reflections from our wider X-ray study are included although more are cited in the text.

The investigated samples were cut from dislocation-free Cz Si single crystals of low carbon concentration ($C_s < 10^{16}$ cm^{-3}) and with varying concentrations of interstitial oxygen atoms (O_i) ranging from 6.85×10^{17} cm^{-3} to 8.50×10^{17} cm^{-3}. The samples were [001] or [111]-oriented, and their thickness varied between 265 μm and 330 μm. Sample A was intentionally doped with phosphorus to obtain n-type material with a resistivity of 5 Ω cm. The remaining samples (B and C) were doped with differing concentrations of boron; as a result, they were of p-type and had resistivities between 4 Ω cm and 18 Ω cm.

Figure 2. (Facing page.) Series of Lang section topographs for a [111] oriented Fz Si crystal. Initial oxygen concentration 0.1×10^{17} cm^{-3}, n-type, resistivity 60 Ω cm, thickness 560 μm. 404 type reflection, $MoK_{\alpha 1}$ radiation. The sample was annealed at 1473 K for 5 min under a hydrostatic pressure of 0.87 GPa. A series of topographs was obtained by successive translation of the sample across the primary beam. The computer simulations were obtained by solving the Takagi–Taupin equations (Takagi 1962, 1969; Taupin 1964) for a spherically symmetric strain field (Lefeld-Sosnowska & Gronkowski 1989). The depth of the defects from the entrance surface was 50 μm. Relative positions of the defects inside the Borrmann triangle (distance from mid-point of Borrmann triangle with '−' indicating to the left and '+' indicating to the right): (*a*) −60 μm; (*b*) −40 μm; (*c*) −10 μm; (*d*) +20 μm; (*e*) +40 μm.

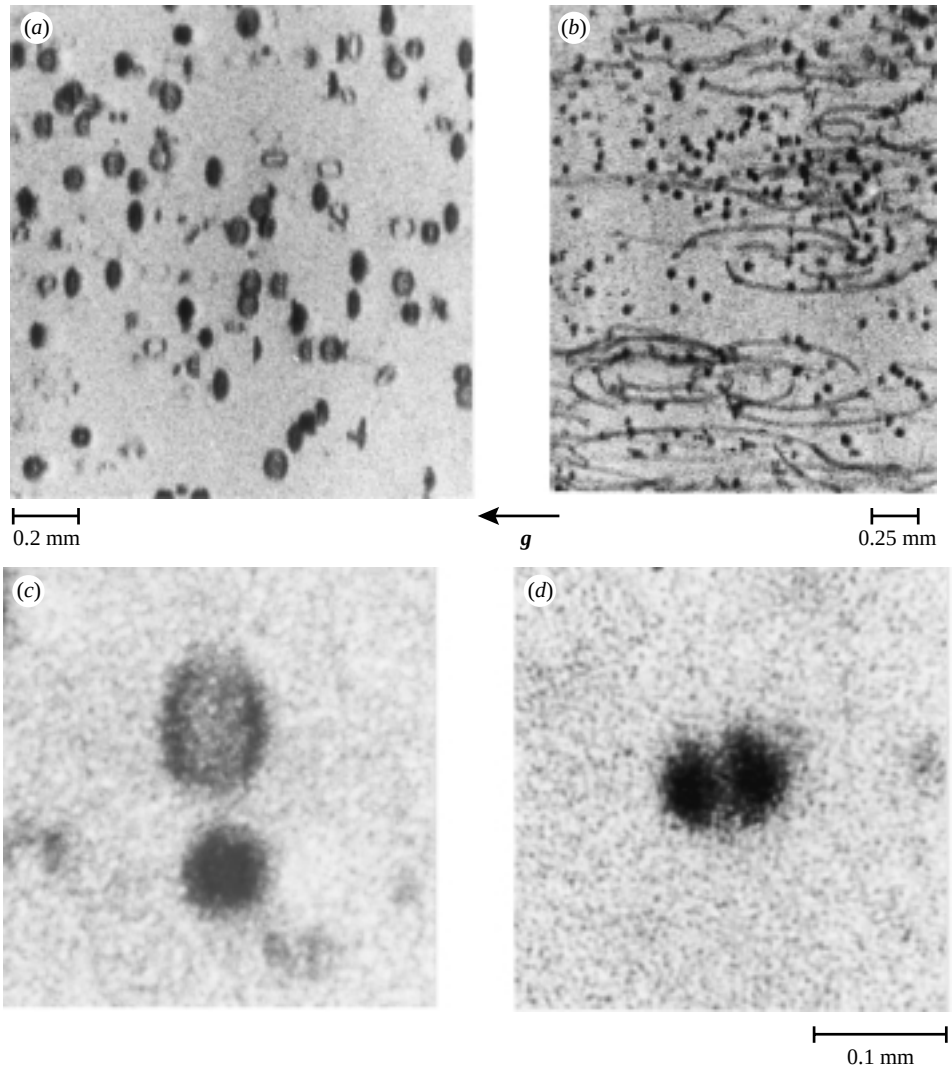

Figure 3. Lang traverse topograhs of two Cz grown [001]-oriented n-type silicon samples ((*a*) and (*b*)) after a two-step heat treatment. $MoK_{\alpha 1}$ radiation, 220 reflection, Ilford G5 50 μm emulsion. Initial oxygen concentration in both samples 8.5×10^{17} cm^{-3}. (*a*) Anneal step 1–75 min at 1173 K, step 2–8 h at 1423 K. (*b*) Anneal step 1–75 min at 1173 K, step 2–10 h at 1423 K. Numerous microdefects can be seen on both samples. On sample (*b*), curved dislocation lines anchored on precipitates are present. Higher photographic magnification (160×) of single microdefects clearly shows characteristic contrast of prismatic loops (*c*) and spherical precipitates with a line of no contrast perpendicular to the diffracting vector. (*d*) Average size of microdefects estimated at about 90 μm (Lefeld-Sosnowska *et al*. 1995).

(*b*) *Thermal treatment*

Two different annealing processes were applied to the samples. In the first, the nucleation was carried out during isothermal annealing at 1023 K for 4 h (samples A and B) followed by annealing at 1323 K for 1 h and at 1423 K for 4 h. In the sec-

ond, nucleation was realized under gradually increasing temperature (by 1 K min^{-1}) increasing from 1023 K up to 1323 K, then samples were annealed isothermally at 1323 K for 1 h and at 1423 K for 4 h (sample C).

(*c*) *Experiment*

Four different experimental techniques—X-ray Lang traverse topography (Lang 1958, 1959*a*, *b*), X-ray section topography (Lang 1957), Fourier transform infrared absorption spectroscopy (FTIR), and transmission electron microscopy (TEM)—were applied in order to characterize the defects formed during the annealing processes. We will focus mainly on results from X-ray experiments.

All of our X-ray measurements were done using $\mathrm{MoK}_{\alpha 1}$ radiation. Lang traverse topographs were taken with 220 and 224 symmetric reflections. Section topographs for the [001] oriented samples were taken with symmetric 440 and 660 reflections as well as with asymmetric 333, 444 and 335 reflections. For the [111] oriented samples, symmetric 224 and 448 reflections, as well as asymmetric 333, 004 and 117 reflections, were used. The topographs were recorded on Ilford L4 50 μm nuclear emulsions.

(*d*) *X-ray Lang traverse topography*

The Lang topographs of the samples annealed isothermally at 1023 K (A and B) are shown in figure 4. The spotty contrast, which is characteristic of thermally introduced precipitates and microdefects, is observed only for wafer A with the highest initial oxygen concentration. Sample B shows only a couple of microdefects of sufficient size to be recorded by this method. On the other hand, on all topographs for gradually annealed samples (e.g. sample C, figure 5) one can see the contrast of many microdefects with different concentrations and dimensions, even for low oxygen concentrations. Sample C is an example of the low-density case.

(*e*) *X-ray section topography*

Some examples of the section topographs obtained for isothermally and gradually annealed samples are shown in figure 6 (samples A and B) and figure 7 (sample C), respectively. The Kato interference fringes are readily recognized on all topographs (for either symmetric or asymmetric reflections) for samples with the lowest content of oxygen in as-grown crystals (e.g. sample B, figure 6). The section topographs of sample C (with slightly higher initial oxygen concentration then sample B and lower than sample A) exhibit the distinct interference structure and a clear 'margin effect' only for symmetrical reflections. In the 333 and 004 asymmetrical reflections, only weak fringes, with no margin effect were recorded. Neither interference structure nor margin effect can be seen in highly asymmetric 335 or 117 reflections.

Sample A, which has the highest oxygen concentration as well as the highest density of large-size microdefects, shows a good deal of standard interference structure for symmetric 660-type and slightly asymmetric 333-type reflections. For highly asymmetric 335 reflections, only a weak margin effect was recorded.

4. Discussion and conclusions

Some of the annealing methods used to remove unwanted species from all, or specific parts, of the silicon wafers (e.g. gradual anneal) appeared to be more effective in

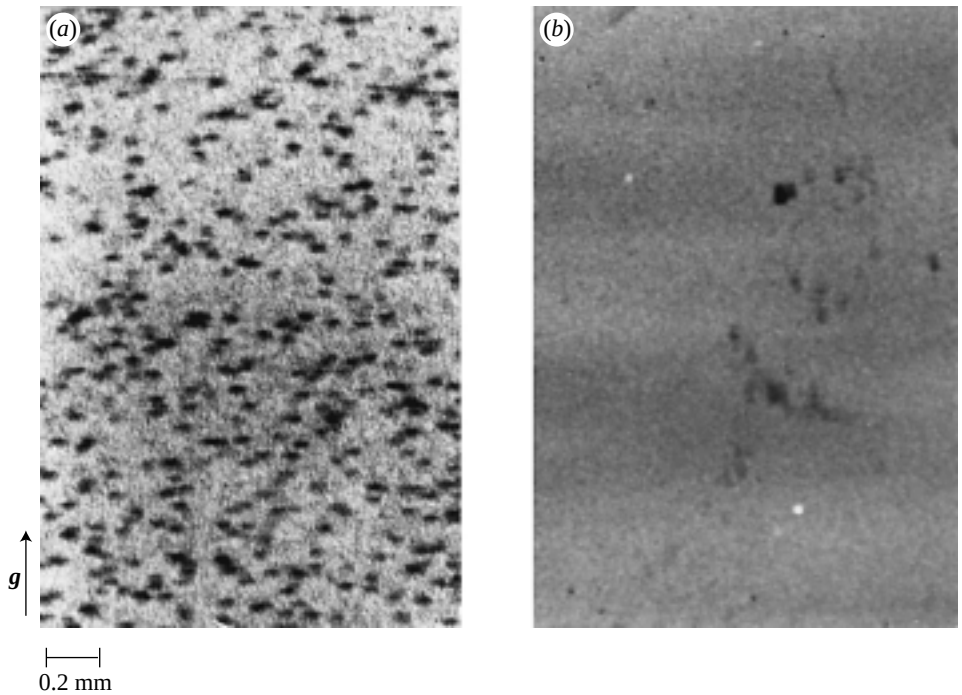

Figure 4. [001] silicon crystals after three-step annealing with the first step isothermal at 1023 K. Lang traverse topographs, 220 reflection, $MoK_{\alpha 1}$ radiation. (*a*) Sample A, initial oxygen concentration 8.5×10^{17} cm^{-3}, n-type sample, phosphorus concentration 10^{15} cm^{-3}, resistivity 5 Ω cm, thickness 290 μm. (*b*) Sample B, initial oxygen concentration 7.15×10^{17} cm^{-3}, p-type sample, boron concentration 3.5×10^{15} cm^{-3}, resistivity 4 Ω cm, thickness 330 μm. The higher initial oxygen concentration in sample A is a source of large size microdefects of substantial density in this sample. Average defect size 30 μm.

such applications in terms of time. This has direct impact on production yield and detailed analysis of all parameters involved in such processes is of prime importance to the electronics industry.

Lang traverse topographs of all samples investigated, of which A, B and C are only examples chosen for this paper, show that a high oxygen concentration played the main role in the formation of the microdefects with sizes recordable by this technique. Although oxygen was not the only foreign atom incorporated into the silicon crystals, the intentional dopants boron and phosphorus have densities of three orders of magnitudes lower, but the presence of oxygen was prevalent. The second important factor was the type of annealing process applied. A gradual increase in temperature during the nucleation phase (the first step of the annealing process in one of our procedures) was equally important. Silicon crystals with similar initial concentrations of oxygen (with the values on the lower side) developed large precipitates only for the gradual anneal. When the oxygen concentration is high enough (*ca.* 10^{18} cm^{-3} in our case), both types of annealing process produce large microdefects. The role of the annealing process and concentration of oxygen of the size of precipitates can be easily and simply concluded from Lang traverse topography.

Section topography presented us with different types of problem to be solved. The

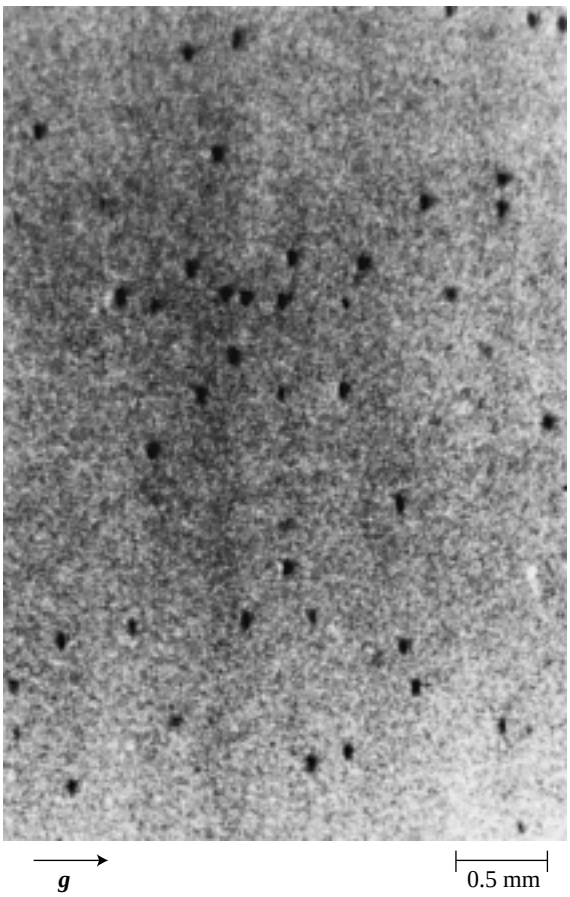

Figure 5. [001] silicon crystal after three-step annealing with the first step gradual (1 K min^{-1}). Lang traverse topograph, 220 reflection, $\mathrm{MoK}_{\alpha 1}$ radiation. Sample C, initial oxygen concentration 7.5×10^{17} cm^{-3}, p-type sample, boron concentration 0.73×10^{15} cm^{-3}, resistivity 18 Ω cm, thickness 290 μm. Medium density of large-scale microdefects recorded. Average defect size estimated at 50 μm.

destruction of interference fringes due to the presence of large densities of microdefects with considerable sizes is already known (Patrick *et al*. 1979; Kishino *et al*. 1979; Stephenson 1992). Sample A (figure 6) is a good example in which individual images of microdefects are still recognizable.

The Kato fringes are influenced by macroscopic deformations due to statistical distributions of small defects (Kato 1980; Stephenson 1990; Sugita *et al*. 1987; Iida *et al*. 1988; Li *et al*. 1994). Their presence in large quantities changes the structure factor of the given reflection $\boldsymbol{H} = (h, k, l)$ by the so-called static Debye–Waller (SDW) factor $E_H = \exp(-L_H)$, where $L_H = \frac{1}{2}(\boldsymbol{H} \cdot \langle \boldsymbol{U} \rangle)^2$ ($\langle \boldsymbol{U} \rangle$ is the average displacement of the crystal lattice introduced by the defects). The SDW depends, therefore, on the characteristics of the defects: their type, strain field parameters and concentration. On the other hand, the period of the Kato fringes scales with E_H^{-1} and their contrast scales with E_H^{-2} (Kato 1980). Therefore, when the average fault vector $\boldsymbol{U}$ is large,

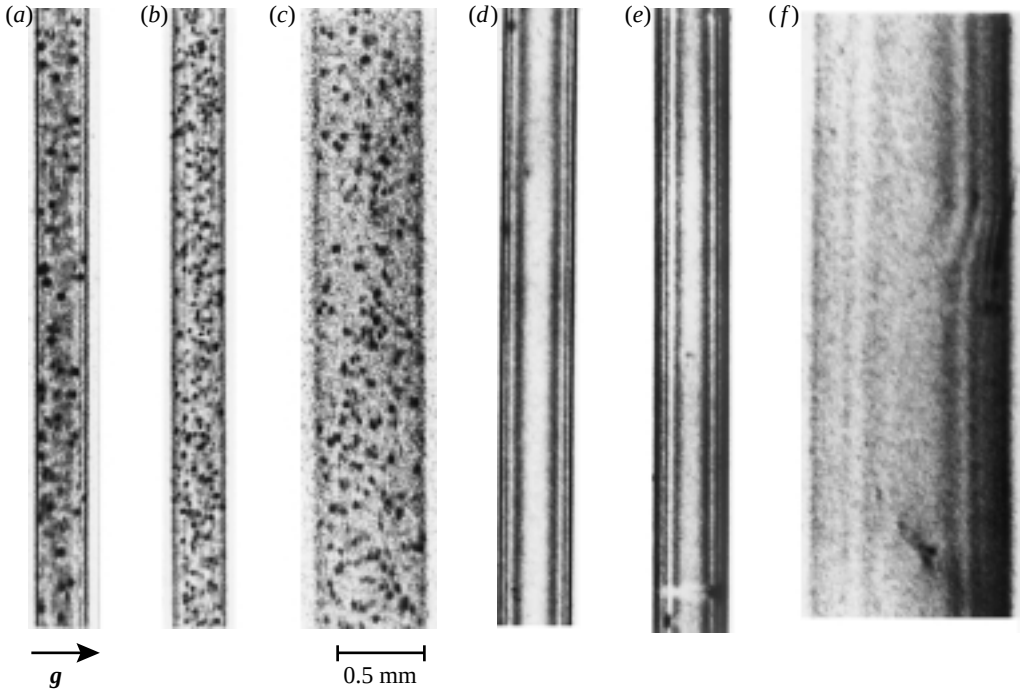

Figure 6. Lang section topography of samples A and B (see figure 4 for details). $MoK_{\alpha 1}$ radiation; (*a*) sample A, symmetric 660 reflection, (*b*) sample A, asymmetric 333 reflection, (*c*) sample A, highly asymmetric 335 reflection. (*d*) Sample B, symmetric 660 reflection, (*e*) sample B, asymmetric 333 reflection, (*f*) sample B, highly asymmetric 335 reflection.

i.e. the SDW becomes substantially smaller than 1, the Kato fringes are not resolved, suggesting that the sample is too deformed for the dynamical diffraction theory to be applicable. That is the case in sample A.

For some other samples (B is an example) the Kato fringes are visible, indicating that their total macroscopic deformation is rather small, implying that either the microdefects are virtually non-existent or their size is too small to cause any significant disturbance of the wave fields inside the Borrmann triangle. Sample C is an intermediary case in this respect; the fringes are distinct only for the least-sensitive symmetric reflection. The highly asymmetric case for sample C, however, shows that there must be a difference in size or density of microdefects in comparison with sample B, where the initial oxygen concentration was similar. We already know that the annealing process used for sample C (gradual) creates more and bigger microdefects. The gradual annealing process may lead to relatively larger microdefect sizes on a scale not resolved on Lang topograhs. This was confirmed by transmission electron microscopy, where sample B showed defect sizes well below 500 nm and sample C showed defect sizes up to 2 μm. We can conclude that one can indirectly record, via observation of the destruction of the interference pattern on the section topograph, the presence of defects, which do not manifest themselves as standard defect images on traverse topographs and are below the resolution of the photographic emulsion. It suggests that highly asymmetric reflections are more sensitive and, therefore, are more suitable than symmetric reflections for observing the influence of very small

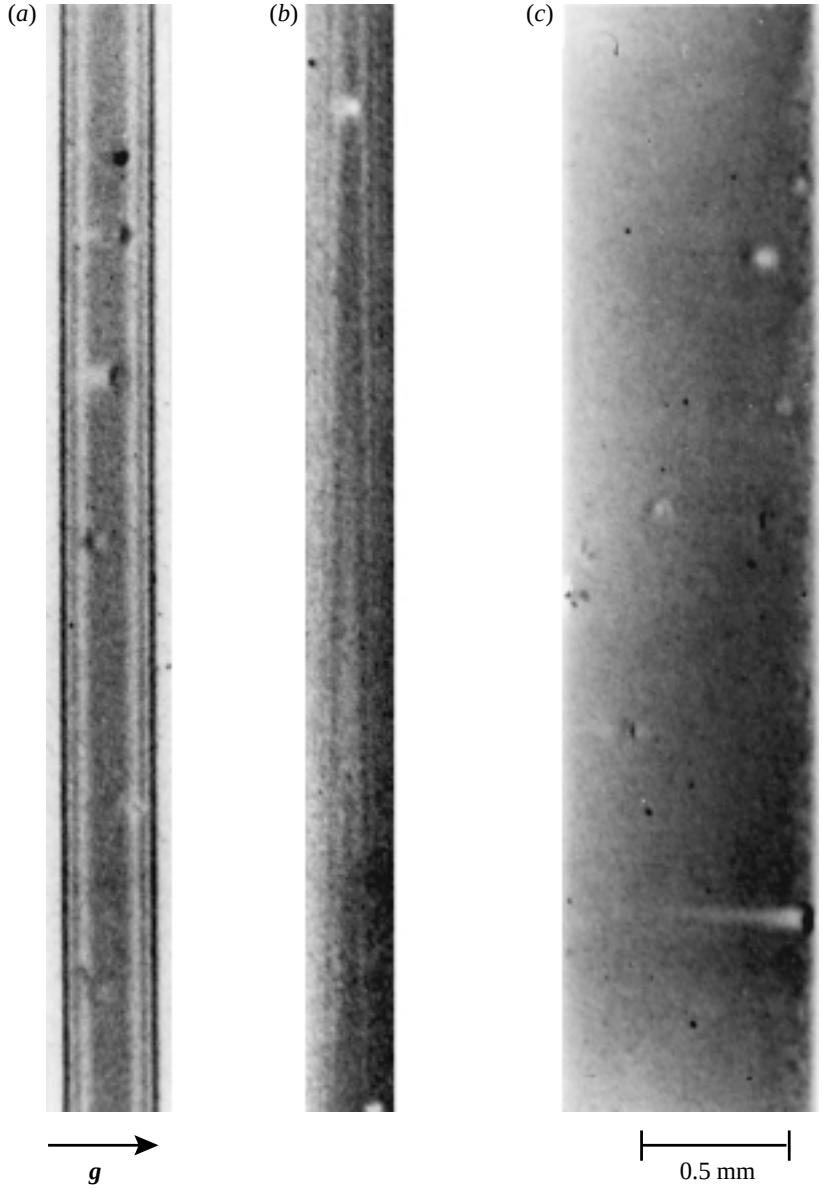

Figure 7. Lang section topography of sample C (see figure 5 for details). $MoK_{\alpha 1}$ radiation; (*a*) symmetric 660 reflection, (*b*) asymmetric 333 reflection, (*c*) highly asymmetric 335 reflection.

defects with weak distortion fields. The sensitivity of the symmetric reflections can be significantly increased by taking the topographs with very high reflection order. Such experiments were recently performed by Iida *et al.* (1998), where reflections up to order 12 with very short wavelength, selected from the synchrotron radiation spectrum, were used.

The technical assistance of J. Bondziul and T. Czekalski in preparing this paper is much appreciated.

References

Authier, A. 1975 Lecture A12. *Int. Summer School on X-ray Dynamical Theory and Topography, August 18–26, Limoges, France.*

Borghesi, A., Pivac, B., Sassella, A. & Stella, A. 1995 *J. Appl. Phys.* **77**, 4169–4244.

Bowen, D. K. & Tanner, B. K. 1998 *High resolution X-ray diffractometry and topography.* London: Taylor and Francis.

Chikawa, J. & Shirai, S. 1977 *J. Cryst. Growth* **39**, 328–340.

De Kock, A. J. R. 1970 *Appl. Phys. Lett.* **16**, 100–102.

De Kock, A. J. R. 1973 *Philips Res. Rep.* Suppl. no. 1.

De Kock, A. J. R. & van de Wijgert, W. M. 1980*a* *J. Cryst. Growth* **49**, 718–734.

De Kock, A. J. R. & van de Wijgert, W. M. 1980*b* *J. Cryst. Growth* **53**, 563–573.

De Kock, A. J. R., Roksnoer, P. J. & Boonen, P. G. T. 1974 *J. Cryst. Growth* **22**, 311–320.

De Kock, A. J. R., Roksnoer, P. J. & Boonen, P. G. T. 1975*a* *J. Cryst. Growth* **28**, 125–137.

De Kock, A. J. R., Roksnoer, P. J. & Boonen, P. G. T. 1975*b* *J. Cryst. Growth* **30**, 279–294.

De Kock, A. J. R., Stacy, W. T. & van de Wijgert, W. M. 1979 *Appl. Phys. Lett.* **34**, 611–613.

Föll, H., Gösele, U. & Kolbesen, B. O. 1981 *J. Cryst. Growth* **52**, 901–916.

Freeland, P. E., Jackson, C. W., Lowe, C. W. & Patel, J. R. 1977 *Appl. Phys. Lett.* **31**, 31–33.

Green, G. S., Cui, S. F. & Tanner, B. K. 1990 *Phil. Mag.* A **61**, 23–33.

Holland, A. J. & Tanner, B. K. 1995 *J. Phys.* D **29**, A27–A32.

Holland, A. J., Green, G. S., Tanner, B. K. & Mai, Z. H. 1991 *Mater. Res. Soc. Symp.* **209**, 475–480.

Iida, S., Sugiyama, H., Sugita, Y. & Kawata, H. 1988 *Japan. J. Appl. Phys.* **27**, 1081–1087.

Iida, S., Takeno, H., Sugita, Y. & Kawata, H. 1990 *Japan. J. Appl. Phys.* **29**, 970–973.

Iida, S., Aoki, Y., Okitsu, K., Sugita, Y., Kawata, H. & Abe, T. 1998 *Japan. J. Appl. Phys.* **37**, 241–246.

Jung, J. & Lefeld-Sosnowska, M. 1984 *Phil. Mag.* A **50**, 233–255.

Kato, N. 1980 *Acta Crystallogr.* A **36**, 763–769.

Kishino, S., Kanamori, M., Yoshihiro, N., Tajima, M. & Iizuka, T. 1979 *J. Appl. Phys.* **50**, 8240–8243.

Kung, C. Y. 1989 *J. Appl. Phys.* **65**, 4654–4665.

Lang, A. R. 1957 *Acta Metall.* **5**, 358–364.

Lang, A. R. 1958 *J. Appl. Phys.* **29**, 597–598.

Lang, A. R. 1959*a* *J. Appl. Phys.* **30**, 1748–1755.

Lang, A. R. 1959*b* *Acta Crystallogr.* **12**, 249–250.

Lefeld-Sosnowska, M. 1985 In *Defects in Crystals. Proc. 7th Int. School on Defects in Crystals, Szczyrk, Poland, 23–30 May* (ed. E. Mizera), pp. 76–88. World Scientific.

Lefeld-Sosnowska, M. & Gronkowski, J. 1989 *Coll. Abstr. 12th Eur. Cryst. Congress, Moscow, USSR*, vol. 29.

Lefeld-Sosnowska, M., Gronkowski, J. & Andrejczuk, A. 1988 In *Defects in Crystals. Proc. 8th Int. School on Defects in Crystals, Szczyrk, Poland, 22–29 May* (ed. E. Mizera), pp. 91–96. World Scientific.

Lefeld-Sosnowska, M., Gronkowski, J. & Kowalski, G. 1995 *J. Phys.* D **28**, A42–A46.

Lefeld-Sosnowska, M., Gronkowski, J., Kowalski, G. & Surma, B. 1996*a* *Coll. Abstr. 3rd Eur. Symp. on X-Ray Topography and High-Resolution Diffraction, X-Top '96, 22–24 April 1996, Palermo, Italy*, vol. 124.

Lefeld-Sosnowska, M., Gronkowski, J., Kowalski, G. & Surma, B. 1996*b* *Coll. Abstr. 3rd Int. School and Symposium on Synchrotron Radiation in Natural Science ISSRNS'96, Jaszowiec, Poland*, vol. 87.

Li, M., Mai, Z.-H. & Cui, S.-F. 1994 *Acta Crystallogr.* A **50**, 725–730.

Mai, Z. H., Cui, S.-F., Wang, C. Y., Wu, L. S., Li, H. P., Chen, G. Y. & Zhou, S. R. 1990 *Mod. Phys. Lett.* B **4**, 625–630.

Matsui, J. & Kawamura, T. 1972 *Japan. J. Appl. Phys.* **11**, 197–205.

Okitsu, K., Iida, S., Sugita, Y., Takeno, H., Yagou, Y. & Kawata, H. 1992 *Japan. J. Appl. Phys.* **31**, 3779–3785.

Patel, J. R. 1973 *J. Appl. Phys.* **44**, 3903–3906.

Patel, J. R. & Authier, A. 1975 *J. Appl. Phys.* **46**, 118–125.

Patel, J. R. & Batterman, B. W. 1963 *J. Appl. Phys.* **34**, 2716–2721.

Patel, J. R., Jackson, K. A. & Reiss, H. 1977 *J. Appl. Phys.* **48**, 5279–5288.

Patrick, W., Hearn, E., Westdorp, W. & Bohg, A. 1979 *J. Appl. Phys.* **50**, 7156–7164.

Ramachandran, G. N. 1944 *Proc. Indian Acad. Sci.* A **19**, 280–292.

Roksnoer, P. J. 1984 *J. Cryst. Growth* **68**, 596–612.

Roksnoer, P. J. & van de Boom, M. M. B. 1981 *J. Cryst. Growth* **53**, 563–573.

Roksnoer, P. J., Bartels, W. J. & Bulle, C. W. T. 1976 *J. Cryst. Growth* **35**, 245–248.

Rozgonyi, G. A. & Jaccodine, R. J. 1983 In *Defects in semiconductors* (ed. S. Mahajan & J. W. Corbett). *Proc. Mater. Res. Soc. Symp.*, 2nd edn, vol. 14, pp. 181–185. Amsterdam: North-Holland.

Stephenson, J. D. 1990 *Physica Status Solidi* A **122**, 171–186.

Stephenson, J. D. 1992 *Physica Status Solidi* A **130**, 75–82.

Sugita, Y., Sugiyama, H., Iida, S. & Kawata, H. 1987 *Japan J. Appl. Phys.* **26**, 1903–1906.

Surma, B. 1988 Institute of Electronic Materials, Technology Report, Warsaw.

Takagi, S. 1962 *Acta Crystallogr.* **15**, 1311–1312.

Takagi, S. 1969 *J. Phys. Soc. Japan* **26**, 1239–1252.

Tanner, B. K. 1976 *X-ray diffraction topography.* Pergamon.

Taupin, D. 1964 *Bull. Soc. Franç. Minér. Crist.* **87**, 469–511.

Tsuya, H., Kondo, Y. & Kanamori, M. 1983 *Japan. J. Appl. Phys.* **22**, L16–L18.

Yamamoto, K., Kishino, S., Matsushita, Y. & Iizuka, T. 1980 *Appl. Phys. Lett.* **36**, 195–197.

Yang, K., Carle, J. & Kleinhenz, R. 1987 *J. Appl. Phys.* **62**, 4890–4896.

Zulehner, W. 1989 *Landolt–Börnstein neue serie* (ed. O. Madelung & M. Schulz), vol. III/22B, pp. 391–438. Springer.